Dalton Transactions

ROYAL SOCIETY OF CHEMISTRY

PAPER

View Article Online
View Journal | View Issue

Check for updates

Cite this: *Dalton Trans.*, 2025, **54**, 17825

Spin-crossover semiconductors based on homoleptic tris-diimine Fe(II) complexes with fractionally charged TCNQ$^{\bullet\delta-}$ anions

Botagoz Amanyazova,[a,b] Sandugash Yergeshbayeva,†[a] Eun Sang Choi,[c] Rakhmetulla Erkasov[b] and Michael Shatruk *[a,d]

Received 3rd October 2025,
Accepted 1st November 2025

DOI: 10.1039/d5dt02365c

rsc.li/dalton

Two hybrid inorganic–organic materials were obtained by crystallization of metal cationic complexes $[FeL_3]^{2+}$ with fractionally charged organic radical anions TCNQ$^{\bullet\delta-}$, where L = 3-(thiazol-2-yl)pyrazole (3tpH) or 4,4′-bithiazole (4bt) and TCNQ = 7,7,8,8-tetracyanoquinodimethane. Crystal structure determination revealed the formula $[FeL_3](TCNQ)_3$ for each complex, indicating the average charge of –2/3 per each TCNQ unit. The crystal packing of each complex features layers of the $[FeL_3]^{2+}$ cations alternating with layers of 1D stacks of the TCNQ$^{\bullet\delta-}$ anions. Magnetic measurements revealed a predominantly high-spin state of the Fe(II) ion for $[Fe(3tpH)_3](TCNQ)_3$ and a gradual spin crossover for $[Fe(4bt)_3](TCNQ)_3$. Transport measurements showed that both materials behave as semiconductors, with room-temperature conductivity values equal to 2.0×10^{-3} S cm^{-1} and 2.0×10^{-2} S cm^{-1}, respectively. The substantially higher conductivity of the bt-containing material was traced to the more uniform charge distribution over the TCNQ units, as established by the crystal structure analysis. Overall, this study provides insight into design principles for solvent-free crystal structures that combine spin crossover with electrical conductivity.

Open Access Article. Published on 05 November 2025. Downloaded on 1/23/2026 10:23:51 AM.
This article is licensed under a Creative Commons Attribution-NonCommercial 3.0 Unported Licence.

Introduction

Molecular materials that exhibit bistability due to existence in different physical states are of interest for the development of new sensing and switching technologies that leverage the contrast between optical, electric, or magnetic responses of the corresponding states.[1–11] One of the largest groups of such materials is represented by spin-crossover (SCO) complexes of transition metal ions that undergo switching between the low-spin (LS) and high-spin (HS) electronic states with different structural, optical, and magnetic parameters.[12–16] The practical appeal of SCO materials is justified by the broad range of triggers that can be used to switch between the LS and HS states, including temperature, pressure, irradiation with light or X-rays, and application of electric and magnetic fields.[17–21]

One of the active research thrusts aims to combine SCO with another function, to achieve multifunctional materials that could be used in novel applications or as replacement for more costly composite materials in existing technologies.[22–27] In this vein, of particular interest are SCO materials that can exhibit high electric conductivity, placing them in the regime of spin-state switchable conductors or semiconductors.[28–32] This class of materials has been actively developed since early 2000s,[33–37] and the general consensus reached to date suggests a hybrid material approach, as opposed to a single-component design, being effective for achieving high conductivity in a spin-state switching crystalline or polymeric solid. In this vein, cationic SCO complexes were combined with organic counter anions known to provide effective charge transport pathways in organic conductors.[34–39] Embedding bistable SCO nanoparticles in a conducting polymer matrix was also demonstrated as an appealing alternative approach.[40,41]

We and other groups have used the well-known organic acceptor 7,7,8,8-tetracyanoquinodimethane (TCNQ) as a component that imparts conductivity to such hybrid materials. Crystallization of cationic SCO complexes of Fe^{II} (electronic configuration $3d^6$, spin states $S = 0$ or 2),[42–46] Fe^{III} ($3d^5$, $S = 1/2$ or 5/2),[47] Co^{II} ($3d^7$, $S = 1/2$ or 3/2),[48,49] and Mn^{III} ($3d^4$, $S = 1$ or 2)[50,51] with fractionally charged TCNQ$^{\bullet\delta-}$ anions ($0 < \delta < 1$) afforded a range of SCO materials, with the conductivities as

[a]*Department of Chemistry and Biochemistry, Florida State University, Tallahassee, FL 32306-4390, USA. E-mail: shatruk@chem.fsu.edu*
[b]*Department of Chemistry, L.N. Gumilyov Eurasian National University, Astana 010008, Kazakhstan*
[c]*National High Magnetic Field Laboratory, Tallahassee, FL 32310, USA*
[d]*FSU Quantum Initiative, Florida State University, Tallahassee, FL 32306, USA*
†Present address: Department of Chemistry, University of Southern California, 840 Downey Way, Los Angeles, CA 90089, USA.

Open Access Article. Published on 05 November 2025. Downloaded on 1/23/2026 10:23:51 AM. This article is licensed under a Creative Commons Attribution-NonCommercial 3.0 Unported Licence.

Table 1 Examples of conducting spin-crossover materials with fractionally charged $TCNQ^{\bullet\delta-}$ anions

Compound[a]	$T_{1/2}$,[b] K	σ,[c] S cm^{-1}
$[Fe^{II}(tpma)(xbim)](ClO_4)(TCNQ)_{1.5}\cdot DMF$[42]	145	2.0×10^{-1}
$[Fe^{II}(tpma)(xbim)](BF_4)(TCNQ)_{1.5}\cdot DMF$[42]	160	n/a
$[Fe^{II}(tpm)_2](TCNQ)_3$[43]	445 (est.)	1.5×10^{-2}
$[Fe_2(bpypz)_2(TCNQ)_2](TCNQ)_2$[46]	337/339	7.7×10^{-1}
$[Fe^{III}(sal_2\text{-trien})](TCNQ)_2\cdot MeOH$[47]	>400	6.0×10^{-1}
$[Fe^{II}(3\text{-bpp})_2](TCNQ)_3\cdot 5MeCN$[44]	230/261[d]	3.1×10^{-3}
$[Fe^{II}(1\text{-bpp})_2](TCNQ)_{3.5}\cdot 3.5MeCN$[45]	234	1.1×10^{-4}
$[Fe^{II}(1\text{-bpp})_2](TCNQ)_4\cdot 4DCE$[45]	166	1.7×10^{-3}
$[Co^{II}(terpy)_2](TCNQ)_3\cdot MeCN$[48]	>400	1.3×10^{-1}
$[Co^{II}(terpy)_2](TCNQ)_4\cdot 3DMF\cdot 0.5H_2O$[49]	>350	3.3×10^{-4}
$[Mn^{III}(5\text{-Cl-salpen})](TCNQ)_{1.5}\cdot 2MeCN$[50]	73/123	1.0×10^{-4}
$[Mn^{III}(3,5\text{-Cl}_2\text{-sal}_2323)](TCNQ)_2$[51]	~300	5.0×10^{-5}

[a] tpma = tris(2-pyridylmethyl)amine; xbim = 1,1′-(α,α′-*o*-xylyl)-2,2′-bisimidazole; tpm = tris(pyrazol-1-yl)-methane; Hbpypz = 3,5-bis(2-pyridyl) pyrazole; H_2sal_2-trien = *N*,*N*′-bis(2-(salicylideneamino)ethyl)-ethane-1,2-diamine; 3-bpp = 2,6-bis(pyrazol-3-yl)pyridine; 1-bpp = 2,6-bis (pyrazol-1-yl)pyridine; terpy = 2,2′;6′,2″-terpyridine; 5-Cl-salpen = *N*,*N*′-bis(3-(2-oxy-5-chlorobenzylideneamino)-propyl)-ethylene-diamine.
[b] The temperature at which the fractions of the HS and LS ions are equal (two values correspond to a hysteretic transition; est. indicates $T_{1/2}$ values estimated by extrapolation above the accessible range).
[c] The conductivity values measured at room-temperature, with the current directed along the TCNQ stacks in the crystal structure.
[d] The SCO was incomplete, with only ~40% HS → LS conversion.

high as 7.7×10^{-1} S cm^{-1} (Table 1). This progress notwithstanding, the stability of these hybrid materials remains a major challenge, because the majority of them contain crystallization solvent that can be readily lost, especially when the material is heated above room temperature.[44] The desolvation can lead to the loss of structural coherence and deterioration of both SCO and transport properties. Only a few materials listed in Table 1 were isolated free of crystallization solvent in their crystal structures. Moreover, the loosely packed structures are likely to decrease the cooperativity of the spin conversion, making the thermally driven SCO appear more gradual,[52–59] as was indeed observed for most of the materials reported to date.

To address these challenges, we have been exploring the use of different cationic Fe(II) complexes, known to exhibit SCO with conventional anions (*e.g.*, ClO_4^- or BF_4^-), in crystallization reactions with the $TCNQ^{\bullet\delta-}$ anions. For example, we showed that increasing the size of the ligand from 3-bpp to bzimpy (2,6-bis(benzimidazol-2′-yl)pyridine) led to more stable complexes $[Fe(bzimpy)_2](TCNQ)_x\cdot n$Solv, which did not lose the crystallization solvent and showed robust semiconducting behavior, although they exist only in the LS state up to 400 K.[44] An alternative approach is to utilize smaller ligands that create a tighter-packed van der Waals surface of the complex, thus encouraging the formation of compact crystal structures without incorporation of solvent molecules. This approach is inspired by the successful synthesis of the solvent-free SCO material $[Fe^{II}(tpm)_2](TCNQ)^3$.[43]

Recently, we reported SCO behavior in homoleptic Fe(II) complexes prepared with thiazole-based ligands, 3-(thiazol-2-yl)pyrazole (3tpH) and 4,4′-bithiazole (4bt) (Scheme 1).[60] The

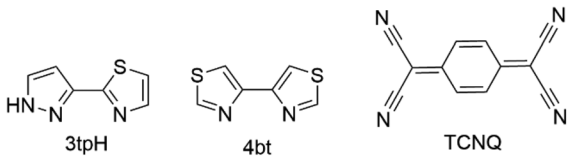

Scheme 1 Organic molecules used in this work.

size and shape of the SCO cations, $[Fe(3tpH)_3]^{2+}$ and $[Fe(4bt)_3]^{2+}$, resemble in some way those observed for the $[Fe^{II}(tpm)_2]^{2+}$ cation. Therefore, we hypothesized that these cations could be crystallized with the $TCNQ^{\bullet\delta-}$ anions to achieve solvent-free hybrid semiconducting materials. Herein, we report the solvent-free structures $[Fe^{II}(3tpH)_3](TCNQ)_3$ (**1**) and $[Fe^{II}(4bt)_3](TCNQ)_3$ (**2**) that corroborate our hypothesis. Although compound **1** exists only in the HS state, compound **2** exhibits gradual and complete SCO with the average crossover temperature of 272 K. Moreover, the synthesis of these materials suggests a strategy for obtaining other solvent-free crystal structures with the potential to combine SCO behavior with electrical conductivity.

Results and discussion

Synthesis

We and others have previously shown that $Et_3NH(TCNQ)_2$ serves as an excellent precursor for the synthesis of transition metal complexes with fractionally charged $TCNQ^{\bullet\delta-}$ anions by simple crystallization with the desired cationic complex of the corresponding metal.[44,61–64] In the present work, crystallization of TCNQ-containing complexes **1** and **2** was achieved by direct layering of a solution of $Et_3NH(TCNQ)_2$ on top of a solution of perchlorate salt of the $[Fe(3tpH)_3]^{2+}$ or $[Fe(4bt)_3]^{2+}$ cation, respectively, which was prepared *in situ*. This procedure afforded high-quality crystals of **1** and **2** as dark-green rods in ~30% yield. Despite the moderate yield, the size and quality of the crystals were considered more important for subsequent magnetic and transport measurements. Most likely, the yield can be improved, but we did not pursue further optimization of these reactions.

Thermogramivetric analysis (TGA, Fig. S1) revealed that both complexes remained thermally stable to ~160 °C, at which point the mass began to decrease slowly and then more rapidly above 200 °C, indicating decomposition of the material. No evident mass loss was observed between 25 °C and 160 °C, suggesting the lack of crystallization solvent in the samples of **1** and **2**, in agreement with the results of crystal structure determination discussed below.

Crystal structures

Single-crystal X-ray diffraction experiments were performed at 90 K and 230 K for **1** and at 100 K, 230 K, and 300 K for **2**, revealing that both crystallize as solvent-free compounds. In general, such solvent-free structures have been relatively rare

 This journal is © The Royal Society of Chemistry 2025

Open Access Article. Published on 05 November 2025. Downloaded on 1/23/2026 10:23:51 AM. This article is licensed under a Creative Commons Attribution-NonCommercial 3.0 Unported Licence.

for the hybrid materials formed by crystallization of SCO complexes with $TCNQ^{\bullet\delta-}$ anions (Table 1).

Both **1** and **2** crystallize in the space group $C2/c$, as observed at all temperatures for which the crystal structure was determined (Table S1). The asymmetric unit (ASU) contains a half of the cationic complex (either $[Fe(3tpH)_3]^{2+}$ or $[Fe(4bt)_3]^{2+}$) and one and a half $TCNQ^{\bullet\delta-}$ anions (Fig. S2). Each cation resides on a 2-fold rotational axis, and each anion is disordered between two configurations generated by ~0.5 Å slippage along the long axis of the molecule (Fig. S3). This disorder, most likely, is correlated with the disorder of the ligands surrounding the Fe center. Thus, in $[Fe(3tpH)_3]^{2+}$, each ligand is disordered over two positions, corresponding to the interchange of the aromatic rings with and without the S atom (Fig. S3a), while in $[Fe(4bt)_3]^{2+}$ two of the ligands show a split position of the S atom in each ring (Fig. S3b).

The Fe^{2+} ion resides in a pseudo-octahedral coordination environment rendered by three 3tpH or three 4bt ligands (Fig. 1). In the case of **1**, the average Fe–N bond length changes from 2.14 Å at 90 K to 2.18 Å at 230 K (Table 2), indicating the predominantly HS state of the Fe^{2+} ion, by comparison to the bond lengths observed for the LS and HS forms of $[Fe(3tpH)_3](ClO_4)_2$ (1.982 Å at 100 K and 2.180 Å at 230 K, respectively).[60] The angular distortion parameter, Σ_{90}, also exhibits only minor changes, increasing from 79(8)° to 89.9(5)°, although the slight decrease in both the average Fe–N bond length and the Σ_{90} parameter upon cooling might indicate an onset of a thermally driven HS → LS conversion.

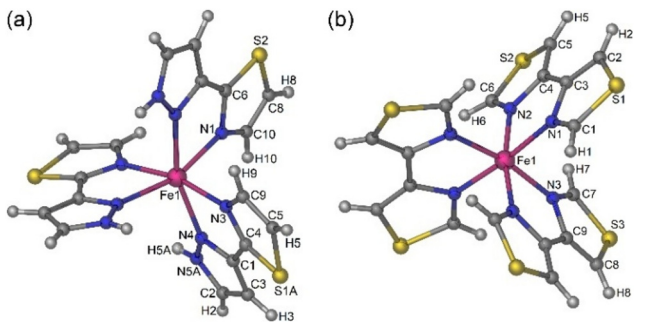

Fig. 1 The cations $[Fe(3tph)_3]^{2+}$ (a) and $[Fe(4bt)_3]^{2+}$ (b) in the crystal structures of **1** and **2**, respectively.

In complex **2**, the average Fe–N bond length of 1.980(1) Å at 100 K indicates the LS state for the Fe^{2+} ion. At 230 K, the average Fe–N distance is only slightly longer, at 2.001(1) Å, but at 300 K it is substantially elongated, to 2.139(1) Å, suggesting predominantly the HS state. The Σ_{90} also shows a pronounced increase, from 51.9(2)° at 100 K to 82.4(4)°, in agreement with the thermally driven conversion from the LS to the HS state. Thus, the comparison of the Fe–N bond lengths and their changes with temperature in complexes **1** and **2** clearly reveals the higher stability of the LS state in the latter, in agreement with the higher ligand-field strength of 4bt in comparison to that of 3tpH, as demonstrated in our previous works.[60,65]

The crystal packing of **1** is characterized by alternating layers of the $[Fe(3tpH)_3]^{2+}$ cations and $TCNQ^{\bullet\delta-}$ anions. The layers are parallel to the bc plane and alternate along the a axis (Fig. 2a). The anionic layers contain columns of the $TCNQ^{\bullet\delta-}$ ions that run along the b axis. In the cationic layers, the most important interactions are van der Waals S···S contacts at 3.520 and 3.682 Å at 230 K (Fig. 2b). No significant π–π stacking interactions are observed. The columns of anions exhibit a stacking sequence [ABBABB...], where A and B indicate symmetry-independent $TCNQ^{\bullet\delta-}$ fragments. The interplanar distances within the column vary non-uniformly, being notably shorter for the B···B than for the A···B separation: 3.11 Å *vs.* 3.35 Å at 230 K (Fig. 2c). The distribution of negative charge on the $TCNQ^{\bullet\delta-}$ fragments was estimated using the Kistenmacher formula,[66] $-\delta = -41.67c/(b + d) + 19.8$, where b, c, and d correspond to interatomic distances in the TCNQ structure (Scheme S1). The charges so calculated were scaled to provide the total charge of −2 per one $TCNQ_A$ and two $TCNQ_B$ units, to compensate for the charge of the $[Fe(3tpH)_3]^{2+}$ cation (see the SI). This procedure yielded charges of −0.56 for $TCNQ_A$ and −0.72 for $TCNQ_B$, showing a rather uniform charge distribution in the anionic column. It should be noted, however, that these calculations were performed only using the more populated fraction of the disordered $TCNQ_B$ fragments. Calculations that used the other part of the disorder or the values averaged over both parts did not yield meaningful results (a similar situation was observed for structure **2** discussed below).

Table 2 Metric parameters of the Fe(II) coordination in the crystal structures of **1** and **2**

Complex	**1**		**2**		
Temperature	90 K	230 K	100 K	230 K	300 K[a]
d(Fe–N), Å	2.10(5) (×2)	2.161(3)	1.977(1) (×2)	1.998(2) (×2)	2.132(3) (×2)
	2.12(4) (×2)	2.178(4)	1.980(1) (×2)	2.002(2) (×2)	2.140(3) (×2)
	2.19(1) (×2)	2.191(4)	1.984(1) (×2)	2.004(2) (×2)	2.146(3) (×2)
d_{av}(Fe–N), Å	2.14(3)	2.177(2)	1.980(1)	2.001(1)	2.139(1)
Σ_{90} (deg)	79(8)	89.8(5)	51.9(2)	57.5(2)	82.4(4)

[a] The Σ_{90} parameter is defined as the sum of absolute deviations of each of the twelve *cis*-octahedral N–Fe–N bond angles from the ideal value of 90°. In complexes with chelating ligands, the HS state is generally characterized by larger values of Σ_{90}, due to stronger distortion from the ideal octahedral coordination.[65]

Open Access Article. Published on 05 November 2025. Downloaded on 1/23/2026 10:23:51 AM.
This article is licensed under a Creative Commons Attribution-NonCommercial 3.0 Unported Licence.

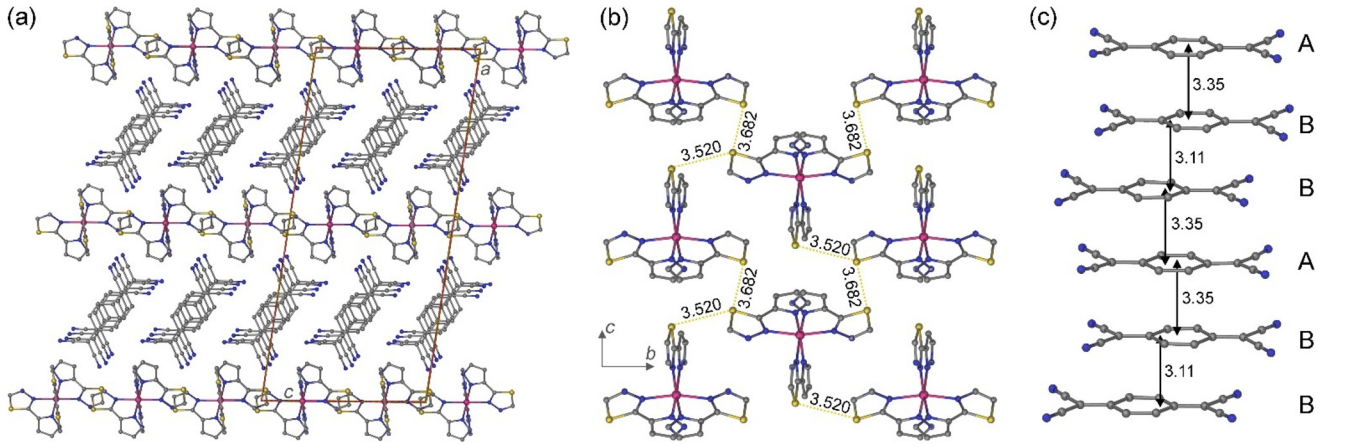

Fig. 2 (a) The crystal packing of **1** viewed parallel to the *ac* plane, with the columns of the $TCNQ^{\bullet\delta-}$ anions propagating perpendicular to the plane of the drawing; the unit cell is shown with solid orange lines. (b) A view of a single layer of the $[Fe(3tpH)_3]^{2+}$ cations in the *bc* plane; the network of intermolecular S···S contacts is shown with dotted yellow lines, with the interatomic distances in Å. (c) The stacking of the $TCNQ^{\bullet\delta-}$ anions, with the interplanar distances shown in Å. Color scheme: Fe = magenta, S = yellow, N = blue, C = gray. The H atoms are omitted for clarity. Only one part of the disorder is shown for each crystallographically disordered fragment.

The crystal packing of **2** is essentially identical to that observed for **1**, with layers of $[Fe(4bt)_3]^{2+}$ cations alternating with layers that contain columns of $TCNQ^{\bullet\delta-}$ anions. The layers are parallel to the *bc* plane and alternate in the *a* direction, while the anionic stacks extend in the *b* direction. In contrast to the structure of **1**, the packing of the cationic complexes appears less efficient, with the nearest S···S distances being as large as 4.49 Å.

Similar to **1**, the crystal packing of **2** contains stacks of $TCNQ^{\bullet\delta-}$ anions with the repeat sequence [ABBABB...], which is characterized by a sequence of interplanar π–π interactions at 3.185, 3.243, 3.315, 3.185, and 3.243 Å. Thus, the difference between the A···B and B···B separations is not as large as in the case of **1**. This might explain the more even charge distribution on the TCNQ units in **2**, −0.68 for $TCNQ_A$ and −0.66 for $TCNQ_B$, which also has reflection in the relative conductivity of these materials (see below).

Magnetic properties

Magnetic susceptibility (χ) measurements were performed on powder samples of **1** and **2**. In the case of **1**, the χT product remained nearly constant, around 3.2 emu K mol^{-1}, upon cooling from 300 K to 150 K but began to decrease gradually at lower temperatures (Fig. 3). The higher-temperature χT value is characteristic of the HS Fe(II) ion and consistent with the results of crystal structure analysis (Table 2). We also note that the observed χT values lack the contribution from the $TCNQ^{\bullet\delta-}$ radical anions. This can be explained by the formation of transient singlet states due to pairing of hopping charges in the TCNQ stack.[67]

The decrease in χT at lower temperatures might be attributed to spin–orbit coupling or zero-field splitting, but such effects are usually not very strong for the HS Fe(II) ion and manifest themselves only below ~50 K.[68] Hence, we suggest that this decrease in χT is correlated with the slight decrease in the Fe–N bond lengths and the angular distortion parameter Σ_{90}, suggestive of an onset of the HS to LS conversion.

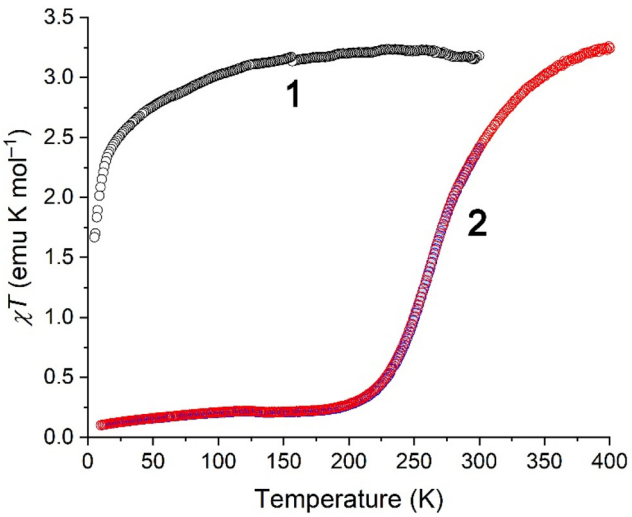

Fig. 3 The temperature dependence of χT measured for a powder sample of **1** in the cooling mode (the black curve) and for a powder sample of **2** in the cooling and heating modes (the blue and red curves, respectively).

Compound **2** showed a gradual and complete SCO in the range from 220 to 400 K. Initially, we cooled the sample from 300 K, observing the decrease in χT from 2.44 emu K mol^{-1} to a plateau of ~0.2 emu K mol^{-1} below 200 K (Fig. 3), which indicates a nearly complete conversion to the LS state. Upon heating from 10 K, the χT *vs.* *T* curve essentially coincided with the one measured in the cooling mode. The gradual increase in χT observed above 220 K continued to 400 K (the highest temperature accessible in our experiment) but the χT began to approach the completion of the SCO, exhibiting a slower increase and reaching the maximum value of 3.26 emu K mol^{-1} at 400 K. The value of the SCO temperature ($T_{1/2}$), at

 This journal is © The Royal Society of Chemistry 2025

Open Access Article. Published on 05 November 2025. Downloaded on 1/23/2026 10:23:51 AM.
This article is licensed under a Creative Commons Attribution-NonCommercial 3.0 Unported Licence.

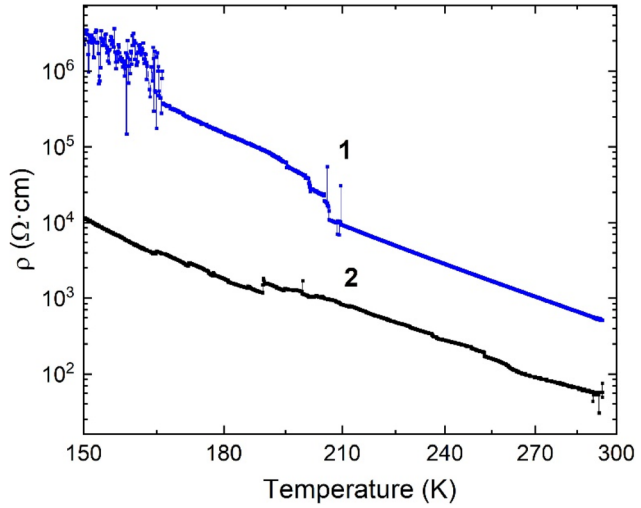

Fig. 4 The temperature dependence of electrical resistivity measured on single-crystal samples of **1** and **2**.

which the fractions of the LS and HS ions are equal, is estimated as 272 K.

These observations for the SCO behavior of **2** are in good agreement with the results of crystal structure analysis (Table 2), where we clearly observed the complete LS state for the Fe(II) ions at 90 K. At 230 K, the average Fe–N bond length and the Σ_{90} parameter are slightly increased relative to those observed at 90 K, which agrees with the onset of the SCO above 220 K observed in the magnetic data. Finally, the 300 K structure exhibits the metric parameters that are closer to the HS state than to the LS state, based on the comparison to the metric parameters of Fe(II) coordination observed for the crystal structure of **1** at 230 K. This structural behavior, again, is well correlated with the magnetic data, where we observe the mid-point of the SCO to occur at $T_{1/2}$ = 272 K.

Transport properties

The temperature dependence of electrical resistance was measured on single crystals of **1** and **2** using the standard 4-probe technique. A smaller size of crystals of **1** necessitated some modification of the 4-probe setup (Fig. S4). The conductivity at 295 K was found to be 2.0×10^{-3} S cm^{-1} for **1** and 2.0×10^{-2} S cm^{-1} for **2**. The higher conductivity of **2** can be attributed to the more uniform charge distribution over the TCNQ units, as observed from the crystal structure analysis discussed earlier. Both compounds showed a gradual increase in resistivity as the temperature was lowered (Fig. 4), in agreement with the semiconducting behavior expected for these materials based on the comparison to similar compounds that combine cationic metal complexes with fractionally charged TCNQ$^{\bullet\delta-}$ anions.[32] The logarithmic resistance showed nearly linear dependence of inverse temperature, allowing us to determine the activation energy for charge hopping as 0.18 eV for **1** and 0.17 eV for **2** (Fig. S5).

Conclusions

This work demonstrates the successful crystallization of Fe(II) cationic complexes with the TCNQ$^{\bullet\delta-}$ radical anions to obtain hybrid materials, one of which exhibits gradual and complete SCO. Importantly, the size and shape of the complex cations is commensurate with the columnar packing of the TCNQ$^{\bullet\delta-}$ anions so that the resulting crystal packing does not include any crystallization solvent. Such situation leads to crystals that are more resistant to disintegration over time, as observed for the majority of other reported materials of this type, which typically crystallize as solvates. The conductivity observed for the complexes reported here places them in the class of hybrid semiconductors, one of which demonstrates spin-state conversion. To increase the conductivity further will require investigation of other types of organic acceptor molecules – *e.g.*, such as substituted TCNQ derivatives – and their structural matching to SCO cations that can be chosen from an extensive library of Fe-, Mn-, or Co-containing SCO complexes.

Experimental

Starting materials

All reactions were performed under inert atmosphere using standard Schlenk techniques. $[Fe(H_2O)_6](ClO_4)_2$ was purchased from Millipore Sigma and used as received. $Et_3NH(TCNQ)_2$,[69] 3tpH,[70] and 4bt[71] were prepared according to the published procedures. Anhydrous commercial solvents were additionally purified by passing through a double-stage drying/purification system (Pure Process Technology). Elemental analyses were carried out by Atlantic Microlab, Inc. (Norcross, GA, USA). Thermogravimetric analysis (TGA) was performed on a TGA-550 thermogravimetric analyzer (TA instruments), with each sample (~2 mg) heated under argon atmosphere from 25 °C to 400 °C at a rate of 10 °C min^{-1}.

$[Fe(3tpH)_3](TCNQ)_3$ (1). A mixture of $[Fe(H_2O)_6](ClO_4)_2$ (36.4 mg, 0.100 mmol) and 3-tpH (45.3 mg, 0.300 mmol) was dissolved in 2 mL of acetonitrile (MeCN) in a Schlenk tube and stirred for 1 h to yield a clear orange solution. On top of this solution was carefully layered a dark-green solution of $Et_3NH(TCNQ)_2$ (76.6 mg, 0.150 mmol) in 9 mL of MeCN, using a thin cannula. The tube was left undisturbed in a purge box filled with nitrogen gas. After 6 days, dark-green rod-shaped crystals of **1** were isolated by filtration and dried by suction. Yield = 30.0 mg (27%). Elem. anal.: calcd (found) for $FeS_3N_{21}C_{54}H_{27}$, %: C, 57.80 (57.01), H, 2.43 (2.21), N, 26.21 (26.04).

$[Fe(4bt)_3](TCNQ)_3$ (2). This complex was synthesized in a manner similar to that described for complex **1**, using 36.4 mg (0.100 mmol) of $[Fe(H_2O)_6](ClO_4)_2$, 67.3 mg (0.400 mmol) of 4-bt, and 76.6 mg (0.150 mmol) of $Et_3NH(TCNQ)_2$ as starting materials. Crystals of **2** were isolated as dark-green rods. Yield = 34.0 mg (29%). Elem. anal.: calcd (found) for $FeC_{54}N_{18}S_6H_{24}$, %: C, 55.28 (55.92), H, 2.06 (1.96), N, 21.49 (22.15).

X-ray crystallography. Single-crystal X-ray diffraction was performed on a Rigaku-Oxford Diffraction Synergy-S diffractometer equipped with a HyPix detector and monochromated

Open Access Article. Published on 05 November 2025. Downloaded on 1/23/2026 10:23:51 AM.
This article is licensed under a Creative Commons Attribution-NonCommercial 3.0 Unported Licence.

Cu-Kα and Mo-Kα radiation sources. In a typical experiment, a single crystal was suspended in Parabar® oil (Hampton Research) and mounted on a cryoloop which was cooled to the desired temperature in an N_2 cold stream. The data set was recorded as ω-scans at 0.5° step width and integrated with the CrysAlis software package.[72] An empirical absorption correction was applied based on spherical harmonics as implemented in the SCALE3 ABSPACK algorithm.[73] The space group was determined with CrysAlis, and the crystal structure solution and refinement were carried out with SHELX[74] using the interface provided by Olex2.[75] The final refinement was performed with anisotropic atomic displacement parameters for all non-hydrogen atoms, except for some atoms of highly disordered anions or solvent molecules, which in such cases were refined isotropically. Full details of crystal structure refinements and the final structural parameters have been deposited with the Cambridge Crystallographic Data Centre (CCDC). The registry numbers and a summary of data collection and refinement parameters are provided in Table S1.

Magnetic measurements. Magnetic properties were measured on polycrystalline samples, using a magnetic property measurement system (MPMS-XL, Quantum Design) equipped with a superconducting quantum interference device (SQUID). Direct-current (DC) magnetic susceptibility was measured in an applied field of 1000 Oe in the 5–400 K temperature range, at cooling/warming rate of 1 K min^{-1} or 2 K min^{-1}. The data were corrected for temperature-independent paramagnetism (TIP), due to the contribution from the excited states of the d^6 Fe^{2+} ion, for diamagnetic contribution from sample holder, and for the intrinsic diamagnetism using tabulated constants.[76]

Transport measurements. Electrical resistance was measured on selected single crystals, with the size of 0.28 × 0.14 × 0.03 mm^3 for **1** and 1.20 × 0.21 × 0.18 mm^3 for **2**. A four-probe measurement setup was used for the latter, while the smaller size of the former necessitated a modified 4-probe configuration. The current was applied parallel to the longest direction of each crystal. The direct current was applied by means of a Keithley 6221 source while a Keithley 2182 nanovoltmeter or a Keithley 6517A electrometer was used to measure the voltage.

Author contributions

Conceptualization, M. S.; methodology, B. A., S. Y., M. S.; validation, B. A., S. Y. M. S.; formal analysis, B. A., S. Y., E. S. C., M. S.; investigation, B. A., S. Y., E. S. C., M. S.; resources, E. S. C., R. E., M. S.; writing – original draft preparation, B. A., S. Y., M. S.; writing – review and editing, E. S. C., M. S.; visualization, B. A., S. Y., M. S.; funding acquisition, R. E., M. S.; supervision, R. E., M. S. All authors have read and agreed to the published version of the manuscript.

Conflicts of interest

There are no conflicts to declare.

Data availability

The data that support the findings of this study are available on request from the corresponding author by sending an email to shatruk@chem.fsu.edu.

Supplementary information (SI): crystal structure refinement and additional crystal structure plots, thermogravimetric data, and estimation of charge distribution on TCNQ units. See DOI: https://doi.org/10.1039/d5dt02365c.

CCDC 2433953–2433957 contain the supplementary crystallographic data for this paper.[77a–e]

Acknowledgements

This work was supported by the U.S. National Science Foundation (awards CHE-2300779 and CHE-1955754). The Rigaku Synergy-S single-crystal X-ray diffractometer used for crystallographic work and the Quantum Design MPMS-3 system used for magnetic measurements were acquired with support of the NSF MRI program (CHE-1828362 and DMR-2216125, respectively). A portion of this work was performed at the National High Magnetic Field Laboratory, which is supported by National Science Foundation Cooperative Agreement No. DMR-2128556 and the State of Florida. The project also used resources provided by the X-ray Crystallography Center (FSU075000XRAY) and the Materials Characterization Laboratory (FSU075000MAC) at the Department of Chemistry and Biochemistry, Florida State University.

References

1 B. T. Worrell, M. K. McBride, G. B. Lyon, L. M. Cox, C. Wang, S. Mavila, C.-H. Lim, H. M. Coley, C. B. Musgrave, Y. Ding and C. N. Bowman, Bistable and photoswitchable states of matter, *Nat. Commun.*, 2018, **9**, 2804.
2 H. Chen and J. F. Stoddart, From molecular to supramolecular electronics, *Nat. Rev. Mater.*, 2021, **6**, 804–828.
3 M. Feng, Z.-Y. Ruan, Y.-C. Chen and M.-L. Tong, Physical stimulus and chemical modulations of bistable molecular magnetic materials, *Chem. Commun.*, 2020, **56**, 13702–13718.
4 Y. Cao, M. Derakhshani, Y. Fang, G. Huang and C. Cao, Bistable structures for advanced functional systems, *Adv. Funct. Mater.*, 2021, **31**, 2106231.
5 J. S. Miller, Bistable electrical, optical, and magnetic behavior in a molecule-based material, *Angew. Chem., Int. Ed.*, 2003, **42**, 27–29.
6 M. Beinhoff, L. D. Bozano, J. C. Scott and K. R. Carter, Design and synthesis of new polymeric materials for organic nonvolatile electrical bistable storage devices: poly(biphenylmethylene)s, *Macromolecules*, 2005, **38**, 4147–4156.

This journal is © The Royal Society of Chemistry 2025

Open Access Article. Published on 05 November 2025. Downloaded on 1/23/2026 10:23:51 AM. This article is licensed under a Creative Commons Attribution-NonCommercial 3.0 Unported Licence.

7 W. R. Dichtel, J. R. Heath and J. F. Stoddart, Designing bistable [2]rotaxanes for molecular electronic devices, *Philos. Trans. R. Soc., A*, 2007, **365**, 1607–1625.
8 S. Di Motta, E. D. Donato, F. Negri, G. Orlandi, D. Fazzi and C. Castiglioni, Resistive molecular memories: influence of molecular parameters on the electrical bistability, *J. Am. Chem. Soc.*, 2009, **131**, 6591–6598.
9 A. C. Fahrenbach, C. J. Bruns, D. Cao and J. F. Stoddart, Ground-state thermodynamics of bistable redox-active donor–acceptor mechanically interlocked molecules, *Acc. Chem. Res.*, 2012, **45**, 1581–1592.
10 Q. Chen, J. Sun, P. Li, I. Hod, P. Z. Moghadam, Z. S. Kean, R. Q. Snurr, J. T. Hupp, O. K. Farha and J. F. Stoddart, A redox-active bistable molecular switch mounted inside a metal–organic framework, *J. Am. Chem. Soc.*, 2016, **138**, 14242–14245.
11 C. Zhou, D. Yang, S. Sensale, P. Sharma, D. Wang, L. Yu, G. Arya, Y. Ke and P. Wang, A bistable and reconfigurable molecular system with encodable bonds, *Sci. Adv.*, 2022, **8**, eade3003.
12 R. Torres-Cavanillas, M. Gavara-Edo and E. Coronado, Bistable spin-crossover nanoparticles for molecular electronics, *Adv. Mater.*, 2024, **36**, 2307718.
13 Z.-S. Yao, Z. Tang and J. Tao, Bistable molecular materials with dynamic structures, *Chem. Commun.*, 2020, **56**, 2071–2086.
14 A. Hauser, J. Jeftić, H. Romstedt, R. Hinek and H. Spiering, Cooperative phenomena and light-induced bistability in iron(II) spin-crossover compounds, *Coord. Chem. Rev.*, 1999, **190–192**, 471–491.
15 P. Gütlich and H. A. Goodwin, Spin crossover - an overall perspective, *Top. Curr. Chem.*, 2004, **233**, 1–47.
16 M. Shatruk, H. Phan, B. A. Chrisostomo and A. Suleimenova, Symmetry-breaking structural phase transitions in spin crossover complexes, *Coord. Chem. Rev.*, 2015, **289**, 62–73.
17 J. F. Létard, P. Guionneau and L. Goux-Capes, Towards spin crossover applications, *Top. Curr. Chem.*, 2004, **235**, 221–249.
18 O. Sato, J. Tao and Y. Z. Zhang, Control of magnetic properties through external stimuli, *Angew. Chem., Int. Ed.*, 2007, **46**, 2152–2187.
19 M. C. Munoz and J. A. Real, Thermo-, piezo-, photo- and chemo-switchable spin crossover iron(II)-metallocyanate based coordination polymers, *Coord. Chem. Rev.*, 2011, **255**, 2068–2093.
20 H. Li and H. Peng, Recent advances in self-assembly of spin crossover materials and their applications, *Curr. Opin. Colloid Interface Sci.*, 2018, **35**, 9–16.
21 E. Coronado, Molecular magnetism: from chemical design to spin control in molecules, materials and devices, *Nat. Rev. Mater.*, 2020, **5**, 87–104.
22 L. Nicole, L. Rozes and C. Sanchez, Integrative approaches to hybrid multifunctional materials: from multidisciplinary research to applied technologies, *Adv. Mater.*, 2010, **22**, 3208–3214.
23 A. D. B. L. Ferreira, P. R. O. Nóvoa and A. T. Marques, Multifunctional material systems: a state-of-the-art review, *Compos. Struct.*, 2016, **151**, 3–35.
24 A. B. Gaspar, V. Ksenofontov, M. Seredyuk and P. Guetlich, Multifunctionality in spin crossover materials, *Coord. Chem. Rev.*, 2005, **249**, 2661–2676.
25 *Multifunctional Molecular Materials*, ed. L. Ouahab, Pan Stanford Publishing, Singapore, 2013.
26 M. Castellano, R. Ruiz-García, J. Cano, J. Ferrando-Soria, E. Pardo, F. R. Fortea-Pérez, S.-E. Stiriba, W. P. Barros, H. O. Stumpf, L. Cañadillas-Delgado, J. Pasán, C. Ruiz-Pérez, G. de Munno, D. Armentano, Y. Journaux, F. Lloret and M. Julve, Metallosupramolecular approach toward multifunctional magnetic devices for molecular spintronics, *Coord. Chem. Rev.*, 2015, **303**, 110–138.
27 D. Pinkowicz, B. Czarnecki, M. Reczyński and M. Arczyński, Multifunctionality in molecular magnetism, *Sci. Prog.*, 2015, **98**, 346–378.
28 M. Wang, Z.-Y. Li, R. Ishikawa and M. Yamashita, Spin crossover and valence tautomerism conductors, *Coord. Chem. Rev.*, 2021, **435**, 213819.
29 O. Sato, Z.-Y. Li, Z.-S. Yao, S. Kang and S. Kanegawa, in *Spin-Crossover Materials: Properties and Applications*, ed. M. A. Halcrow, John Wiley & Sons Ltd., 2013, pp. 303–319.
30 C. Lefter, V. Davesne, L. Salmon, G. Molnár, P. Demont, A. Rotaru and A. Bousseksou, Charge transport and electrical properties of spin crossover materials: towards nanoelectronic and spintronic devices, *Magnetochemistry*, 2016, **2**, 18.
31 V. Rubio-Giménez, S. Tatay and C. Martí-Gastaldo, Electrical conductivity and magnetic bistability in metal–organic frameworks and coordination polymers: charge transport and spin crossover at the nanoscale, *Chem. Soc. Rev.*, 2020, **49**, 5601–5638.
32 Ö. Üngör and M. Shatruk, Transition metal complexes with fractionally charged TCNQ radical anions as structural templates for multifunctional molecular conductors, *Polyhedron*, 2020, **177**, 114254.
33 M. Nakano, N. Fujita, G. E. Matsubayashi and W. Mori, Modified chesnut model for spin-crossover semiconductors $[Fe(acpa)_2](TCNQ)_n$, *Mol. Cryst. Liq. Cryst.*, 2002, **379**, 365–370.
34 S. Dorbes, L. Valade, J. A. Real and C. Faulmann, $[Fe(sal_2\text{-}trien)][Ni(dmit)_2]$: towards switchable spin crossover molecular conductors, *Chem. Commun.*, 2005, 69–71.
35 C. Faulmann, S. Dorbes, B. Garreau de Bonneval, G. Molnar, A. Bousseksou, C. J. Gomez-Garcia, E. Coronado and L. Valade, Towards molecular conductors with a spin-crossover phenomenon: crystal structures, magnetic properties and Mössbauer spectra of [Fe(salten)Mepepy][M(dmit)$_2$] complexes, *Eur. J. Inorg. Chem.*, 2005, 3261–3270.
36 K. Takahashi, H. B. Cui, Y. Okano, H. Kobayashi, Y. Einaga and O. Sato, Electrical conductivity modulation coupled to a high-spin-low-spin conversion in the molecular system $[FeIII(qsal)_2][Ni(dmit)_2]_3{\cdot}CH_3CN{\cdot}H_2O$, *Inorg. Chem.*, 2006, **45**, 5739–5741.

Open Access Article. Published on 05 November 2025. Downloaded on 1/23/2026 10:23:51 AM. This article is licensed under a Creative Commons Attribution-NonCommercial 3.0 Unported Licence.

37 C. Faulmann, K. Jacob, S. Dorbes, S. Lampert, I. Malfant, M. L. Doublet, L. Valade and J. A. Real, Electrical conductivity and spin crossover: a new achievement with a metal bis dithiolene complex, *Inorg. Chem.*, 2007, **46**, 8548–8559.

38 K. Takahashi, H. B. Cui, Y. Okano, H. Kobayashi, H. Mori, H. Tajima, Y. Einaga and O. Sato, Evidence of the chemical uniaxial strain effect on electrical conductivity in the spin-crossover conducting molecular system: [FeIII(qnal)$_2$][Pd(dmit)$_2$]$_5$·Acetone, *J. Am. Chem. Soc.*, 2008, **130**, 6688–6689.

39 Y. N. Shvachko, N. G. Spitsyna, D. V. Starichenko, V. N. Zverev, L. V. Zorina, S. V. Simonov, M. A. Blagov and E. B. Yagubskii, Magnetism, conductivity and spin-spin interactions in layered hybrid structure of anionic radicals [Ni(dmit)$_2$] alternated by iron(III) spin-crossover complex [Fe(III)(3-OMe-Sal$_2$trien)] and ferric moiety precursors, *Molecules*, 2020, **25**, 4922.

40 Y. S. Koo and J. R. Galan-Mascaros, Spin crossover probes confer multistability to organic conducting polymers, *Adv. Mater.*, 2014, **26**, 6785–6789.

41 D. Nieto-Castro, F. A. Garcés-Pineda, A. Moneo-Corcuera, I. Sánchez-Molina and J. R. Galán-Mascarós, Mechanochemical processing of highly conducting organic/inorganic composites exhibiting spin crossover–induced memory effect in their transport properties, *Adv. Funct. Mater.*, 2021, **31**, 2102469.

42 H. Phan, S. M. Benjamin, E. Steven, J. S. Brooks and M. Shatruk, Photomagnetic response in highly conductive iron(II) spin-crossover complexes with TCNQ radicals, *Angew. Chem., Int. Ed.*, 2015, **54**, 823–827.

43 Y. N. Shvachko, D. V. Starichenko, A. V. Korolyov, E. B. Yagubskii, A. I. Kotov, L. I. Buravov, K. A. Lyssenko, V. N. Zverev, S. V. Simonov, L. V. Zorina, O. G. Shakirova and L. G. Lavrenova, The conducting spin-crossover compound combining Fe(II) cation complex with TCNQ in a fractional reduction state, *Inorg. Chem.*, 2016, **55**, 9121–9130.

44 Ö. Üngör, E. S. Choi and M. Shatruk, Optimization of crystal packing in semiconducting spin-crossover materials with fractionally charged TCNQ$^{\delta-}$ anions ($0 < \delta < 1$), *Chem. Sci.*, 2021, **12**, 10765–10779.

45 Ö. Üngör, E. S. Choi and M. Shatruk, Solvent-dependent spin-crossover behavior in semiconducting co-crystals of [Fe(1-bpp)$_2$]$^{2+}$ cations and TCNQ$^{\delta-}$ anions ($0<\delta<1$), *Eur. J. Inorg. Chem.*, 2021, **2021**, 4812–4820.

46 R. Ishikawa, S. Ueno, S. Nifuku, Y. Horii, H. Iguchi, Y. Miyazaki, M. Nakano, S. Hayami, S. Kumagai, K. Katoh, Z.-Y. Li, M. Yamashita and S. Kawata, Simultaneous spin-crossover transition and conductivity switching in a dinuclear iron(II) coordination compound based on 7,7′,8,8′-tetracyano-*p*-quinodimethane, *Chem. – Eur. J.*, 2020, **26**, 1165–1165.

47 Y. N. Shvachko, D. V. Starichenko, A. V. Korolyov, A. I. Kotov, L. I. Buravov, V. N. Zverev, S. V. Simonov, L. V. Zorina and E. B. Yagubskii, *Magnetochemistry*, 2017, **3**, 23.

48 X. Zhang, Z.-X. Wang, H. Xie, M.-X. Li, T. J. Woods and K. R. Dunbar, A cobalt(II) spin-crossover compound with partially charged TCNQ radicals and an anomalous conducting behavior, *Chem. Sci.*, 2016, **7**, 1569–1574.

49 J.-Y. Zhang, L.-J. Su, Q.-J. Guo and J. Tao, Semiconducting spin-crossover cobalt(II) compound with non-integer charge distribution among TCNQ radicals, *Inorg. Chem. Commun.*, 2017, **82**, 39–43.

50 A. V. Kazakova, A. V. Tiunova, D. V. Korchagin, G. V. Shilov, E. B. Yagubskii, V. N. Zverev, S. C. Yang, J.-Y. Lin, J.-F. Lee, O. V. Maximova and A. N. Vasiliev, The first conducting spin-crossover compound combining a MnIII cation complex with electroactive TCNQ demonstrating an abrupt spin transition with a hysteresis of 50 K, *Chem. – Eur. J.*, 2019, **25**, 10204–10213.

51 A. V. Tiunova, D. V. Korchagin, A. V. Kazakova, G. V. Shilov, L. I. Buravov, A. I. Dmitriev, M. V. Zhidkov, V. N. Zverev, E. B. Yagubskii and S. M. Aldoshin, Solvent and dihalide substituent effects on crystal structure, spin-crossover behavior and conductivity of the cationic Mn(III) complexes with electroactive TCNQ counteranions, *Eur. J. Inorg. Chem.*, 2024, **27**, e202300749.

52 K. S. Murray and C. J. Kepert, Cooperativity in spin crossover systems: memory, magnetism and microporosity, *Top. Curr. Chem.*, 2004, **233**, 195–228.

53 M. A. Halcrow, Structure:function relationships in molecular spin-crossover complexes, *Chem. Soc. Rev.*, 2011, **40**, 4119–4142.

54 H. V. Phan, P. Chakraborty, M. M. Chen, Y. M. Calm, K. Kovnir, L. K. Keniley, J. M. Hoyt, E. S. Knowles, C. Besnard, M. W. Meisel, A. Hauser, C. Achim and M. Shatruk, Heteroleptic FeII complexes of 2,2′-biimidazole and its alkylated derivatives: spin-crossover and photomagnetic behavior, *Chem. – Eur. J.*, 2012, **18**, 15805–15815.

55 D. Sertphon, D. J. Harding, P. Harding, K. S. Murray, B. Moubaraki, J. D. Cashion and H. Adams, Anionic tuning of spin crossover in FeIII–quinolylsalicylaldiminate complexes, *Eur. J. Inorg. Chem.*, 2013, 788–795.

56 C. Enachescu and A. Hauser, Study of switching in spin transition compounds within the mechanoelastic model with realistic parameters, *Phys. Chem. Chem. Phys.*, 2016, **18**, 20591–20599.

57 M. Steinert, B. Schneider, S. Dechert, S. Demeshko and F. Meyer, Spin-state versatility in a series of Fe$_4$ [2 × 2] grid complexes: effects of counteranions, lattice solvent, and intramolecular cooperativity, *Inorg. Chem.*, 2016, **55**, 2363–2373.

58 K. A. Zenere, S. G. Duyker, E. Trzop, E. Collet, B. Chan, P. W. Doheny, C. J. Kepert and S. M. Neville, Increasing spin crossover cooperativity in 2D Hofmann-type materials with guest molecule removal, *Chem. Sci.*, 2018, **9**, 5623–5629.

59 S. Yergeshbayeva, J. J. Hrudka, M. Jo, M. Gakiya-Teruya, M. W. Meisel and M. Shatruk, Abrupt spin transition in a heteroleptic Fe(II) complex with pendant naphthalene functionality, *Inorg. Chem.*, 2022, **61**, 11349–11358.

60 M. Jo, B. Amanyazova, S. Yergeshbayeva, M. Gakiya-Teruya, Ö. Üngör, P. Lopez Rivera, N. Jen, E. Lukyanenko,

 This journal is © The Royal Society of Chemistry 2025

Open Access Article. Published on 05 November 2025. Downloaded on 1/23/2026 10:23:51 AM. This article is licensed under a Creative Commons Attribution-NonCommercial 3.0 Unported Licence.

A. V. Kurkin, R. Erkasov, M. W. Meisel, A. Hauser, P. Chakraborty and M. Shatruk, Light-induced spin-state switching in Fe(ii) spin-crossover complexes with thiazole-based chelating ligands, *Dalton Trans.*, 2024, **53**, 10511–10520.

61 H. J. Choi and M. P. Suh, Nickel(II) macrocyclic complexes with long alkyl pendant chain: synthesis, X-ray structure, and anion exchange property in the solid state, *Inorg. Chem.*, 2003, **42**, 1151–1157.

62 L. Ballester, A. M. Gil, A. Gutiérrez, M. F. Perpiñán, M. T. Azcondo, A. E. Sánchez, C. Marzin, G. Tarrago and C. Bellitto, Supramolecular architecture and magnetic properties of copper(II) and mickel(II) porphyrinogen–TCNQ electron-transfer salts, *Chem. – Eur. J.*, 2002, **8**, 2539–2548.

63 Ö. Üngör, H. Phan, E. S. Choi, J. K. Roth and M. Shatruk, Magnetism and electrical conductivity of molecular semiconductor, $[FeII(DMF)_4(TCNQ)_2](TCNQ)_2$, with fractionally charged TCNQ units, *J. Magn. Magn. Mater.*, 2020, **497**, 165984.

64 Ö. Üngör, M. Burrows, T. Liu, M. Bodensteiner, Y. Adhikari, Z. Hua, B. Casas, L. Balicas, P. Xiong and M. Shatruk, Paramagnetic molecular semiconductors combining anisotropic magnetic ions with TCNQ radical anions, *Inorg. Chem.*, 2021, **60**, 10502–10512.

65 H. Phan, J. J. Hrudka, D. Igimbayeva, L. M. Lawson Daku and M. Shatruk, A simple approach for predicting the spin state of homoleptic Fe(II) tris-diimine complexes, *J. Am. Chem. Soc.*, 2017, **139**, 6437–6447.

66 T. J. Kistenmacher, T. J. Emge, A. N. Bloch and D. O. Cowan, Structure of the red, semiconducting form of 4,4′,5,5′-tetramethyl-(,$^{2,2'}$-bi-1,3-diselenole-7,7,8,8-tetracyano-*p*-quinodimethane, TMTSF-TCNQ, *Acta Crystallogr., Sect. B*, 1982, **B38**, 1193–1199.

67 R. G. Kepler, Magnetic properties of a new class of highly conductive organic solids, *J. Chem. Phys.*, 1963, **39**, 3528–3532.

68 M. Shatruk, A. Dragulescu-Andrasi, K. E. Chambers, S. A. Stoian, E. L. Bominaar, C. Achim and K. R. Dunbar, Properties of Prussian blue materials manifested in molecular complexes: observation of cyanide linkage isomerism and spin-crossover behavior in pentanuclear cyanide clusters, *J. Am. Chem. Soc.*, 2007, **129**, 6104–6116.

69 L. R. Melby, R. J. Harder, W. R. Hertler, W. Mahler, R. E. Benson and W. E. Mochel, Substituted quinodimethans. II, Anion-radical derivatives and complexes of 7,7,8,8-tetracyanoquinodimethan, *J. Am. Chem. Soc.*, 1962, **84**, 3374–3387.

70 L. S. Harimanow, K. H. Sugiyarto, D. C. Craig, M. L. Scudder and H. A. Goodwin, Magnetic, spectral and structural aspects of spin transitions in iron(II) complexes of 2-(pyrazol-3-yl)pyridine and 3-(thiazol-2-yl)pyrazole, *Aust. J. Chem.*, 1999, **52**, 109–122.

71 H. Erlenmeyer and M. Erne, On the knowledge of polythiazole compounds, *Helv. Chim. Acta*, 1946, **29**, 275–279.

72 *CrysAlis*, Oxford Diffraction Ltd, Abingdon, England, 2006.

73 *SCALE3 ABSPACK - An Oxford Diffraction program (1.0.4, gui:1.0.3)*, Oxford Diffraction Ltd., Abingdon, England, 2005.

74 G. M. Sheldrick, Crystal structure refinement with SHELXL, *Acta Crystallogr., Sect. C:Struct. Chem.*, 2015, **71**, 3–8.

75 O. V. Dolomanov, L. J. Bourhis, R. J. Gildea, J. A. K. Howard and H. Puschmann, OLEX2: a complete structure solution, refinement and analysis program, *J. Appl. Crystallogr.*, 2009, **42**, 339–341.

76 G. A. Bain and J. F. Berry, Diamagnetic corrections and Pascal's constants, *J. Chem. Educ.*, 2008, **85**, 532–536.

77 (*a*) CCDC 2433953: Experimental Crystal Structure Determination, 2025, DOI: 10.5517/ccdc.csd.cc2mpqmp; (*b*) CCDC 2433954: Experimental Crystal Structure Determination, 2025, DOI: 10.5517/ccdc.csd.cc2mpqnq; (*c*) CCDC 2433955: Experimental Crystal Structure Determination, 2025, DOI: 10.5517/ccdc.csd.cc2mpqpr; (*d*) CCDC 2433956: Experimental Crystal Structure Determination, 2025, DOI: 10.5517/ccdc.csd.cc2mpqqs; (*e*) CCDC 2433957: Experimental Crystal Structure Determination, 2025, DOI: 10.5517/ccdc.csd.cc2mpqrt.